Pergamon

Int. J. Solids Structures Vol. 35, Nos 34–35, pp. 4803–4810, 1998

Printed in Great Britain
0020–7683/98/$—see front matter

PII: S0020–7683(98)00095–X

ACOUSTIC SIGNATURES OF PATCHY SATURATION

JACK DVORKIN† and AMOS NUR
Department of Geophysics, Stanford University, Stanford, CA 94305-2215, U.S.A.

(*Received* 9 *July* 1997; *in revised form* 27 *January* 1998)

Abstract—We consider two saturation patterns in a partially saturated geomaterial. The first is the homogeneous pattern where saturation is the same at the pore scale at any location in the rock. The second is the patchy pattern where a large fully-saturated patch is surrounded by a dry region. In both cases the global saturation in a large volume of the rock is the same. At the same global saturation, the effective acoustic properties of the rock vary depending on the saturation pattern. We offer a practical method for identifying the dominating saturation pattern from dynamic Poisson's ratio obtained from sonic well-log measurements. This method performs well in soft rocks whose acoustic properties are most sensitive to the way fluid is distributed in the pore space.

1. INTRODUCTION AND PROBLEM FORMULATION

The heterogeneous nature of porous rocks and soils often results in the heterogeneity of fluid distribution on scales greater than pore or grain size. In a partially saturated rock two end members of pore fluid arrangement may exist: (a) the fluid is evenly distributed within the pore space, i.e., fluid distribution is homogeneous; and (b) the fluid is arranged in fully saturated patches that are surrounded by dry or partially saturated regions, so that fluid distribution is patchy. These patches may include thousands of grains.

Both types of fluid and pore pressure distribution can occur in several important geological systems: the nature of the oil/gas distribution in a pay zone affects the estimates of reserves, relative permeability, dry-frame elastic properties, and strength. The dry-frame elastic properties are needed for the "fluid substitution" procedure where the velocities in a rock with a new, hypothetical, fluid are calculated from those measured in the rock with the known fluid. The patchy arrangement of ground water is probably common in undersaturated aquifer zones. To determine the details of such patchy arrangements is important for ground water flow calculations and watertable monitoring. Industrial groundwater contaminants in the shallow subsurface may occur in patches, or may be evenly dispersed in the pore space. Determining the arrangement type will help select the remediation technique.

To understand physical reasons for the existence of patchy saturation, let us consider a volume of rock that consists of several sand patches with clay content slightly varying among them. These clay-content variations may have a small effect on the dry-frame elastic moduli but dramatically affect permeability (Yin, 1993) and, therefore, capillary pressure curves. Then, in a state of capillary equilibrium, this elastically homogeneous volume may have a patchy saturation pattern (Knight *et al.*, 1998). Indeed, if capillary pressure is the same for the adjacent patches whose capillary pressure curves are different, these patches can have very different fluid saturations. In the example shown in Fig. 1, at the selected capillary pressure, the low permeability rock is fully water-saturated while the high permeability rock is at a saturation of about 0.3.

Visual proofs that patches form in oil–water and air–water systems in the laboratory are presented by Chatenever and Calhoun (1952) and Cadoret (1993). A question remains whether patchy saturation exists *in situ*.

† Author to whom correspondence should be addressed. Tel.: 001 650 725 9296. Fax: 001 650 725 7344. E-mail: jack@pangea.stanford.edu

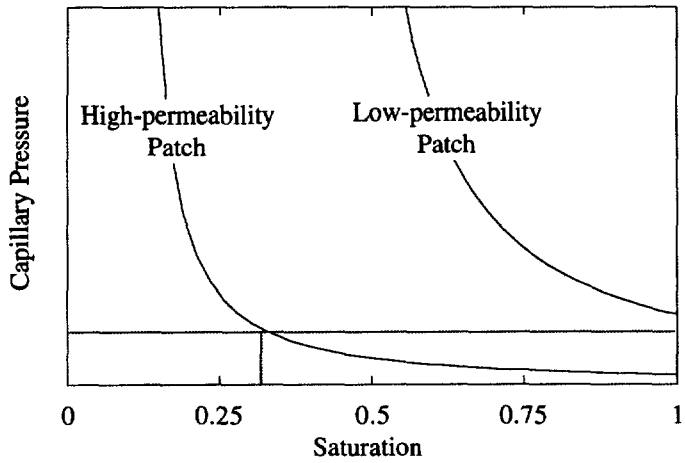

Fig. 1. Schematic capillary pressure curves for a low-permeability and a high-permeability rock. At the same capillary pressure these two neighboring patches may have different saturations. The low-permeability patch is fully saturated whereas the high-permeability patch has a saturation of about 0.3.

To this end we pose a problem to identify the saturation pattern from *in situ* measurements. We assume that the following are available: *P*- and *S*-wave velocity from acoustic measurements, saturation from electrical measurements, bulk density, and porosity from borehole logs. We also assume that the bulk modulus of the mineral phase of the rock, as well as the bulk moduli of the liquid and gas phases are available.

In this work we explore acoustic signatures of patchy saturation at practical well-log frequencies (that vary between 1 and 10 kHz) rather than at ultrasonic laboratory frequencies where artifacts are present related to the unrelaxed behavior of pore fluid (Mavko and Jizba, 1991). An effective elastic medium theory is used to calculate the elastic wave velocities. It is implicitly assumed, therefore, that a patch size has to be smaller than the wavelength in order for the effective medium theory to be applicable.

2. SATURATION AND ACOUSTIC PROPERTIES

The velocity-saturation behavior in a patchy system differs from that in a homogeneous system. Knight *et al.* (1997) estimate this difference theoretically by calculating velocity first in the sand system with the patchy distribution of clay content (see description in Introduction) and then in the same system where all the patches are homogeneously mixed and clay content is uniform in the system (Fig. 2a). This theoretical velocity-saturation behavior is qualitatively similar to the experimental results in Fig. 2b (Cadoret, 1993).

Consider a saturated region of rock where both *P*- and *S*-wave velocities (V_p and V_s, respectively) are available. If this region is sufficiently smaller than the wavelength, it can be treated as an effective medium where wave velocities are related to the effective bulk (K_{sat}) and shear (G_{sat}) moduli as

$$K_{sat} = \rho(V_p^2 - \tfrac{4}{3}V_s^2), \quad G_{sat} = \rho V_s^2, \tag{1}$$

where ρ is the bulk density. According to Gassmann (1951), the dry-frame bulk and shear elastic moduli (K_{dry} and G_{dry}, respectively) are

$$K_{dry} = K_s \frac{1-(1-\phi)K_{sat}/K_s - \phi K_{sat}/K_f}{1+\phi-\phi K_s/K_f - K_{sat}/K_s}, \quad G_{dry} = G_{sat} = G, \tag{2}$$

where ϕ is porosity, and K_s and K_f are the bulk moduli of the mineral phase and pore fluid, respectively.

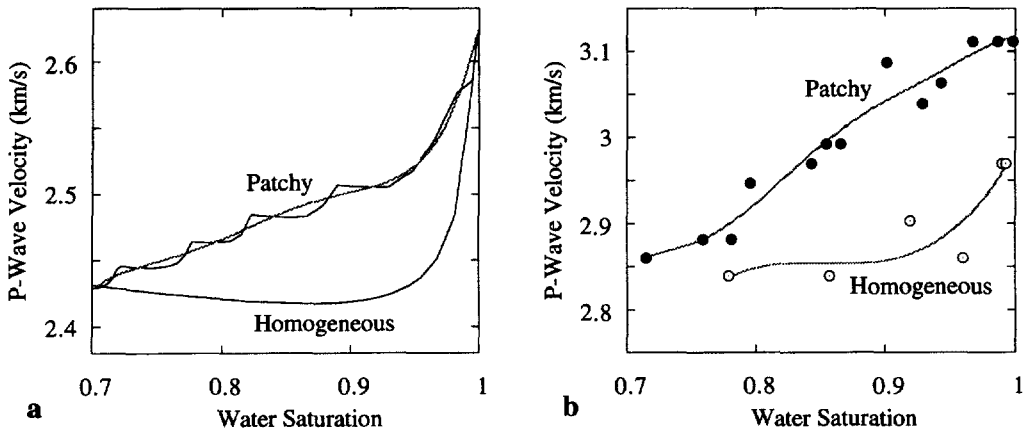

Fig. 2. Velocity vs water saturation for homogeneous and patchy patterns. a. Theoretical results (Knight *et al.*, 1997) for a sand–clay system. Patchy curve is not smooth due to the finite number of patches. It is smoothed by a polynomial fit. b. Experiments of Cadoret (1993) at 50 kHz on a carbonate sample of 30% porosity. The lines are polynomial fits.

The inverse of eqn (2) is

$$K_{sat} = K_s \frac{\phi K_{dry} - (1+\phi)K_f K_{dry}/K_s + K_f}{(1-\phi)K_f + \phi K_s - K_f K_{dry}/K_s}. \tag{3}$$

Equations (2) and (3) are valid at a low frequency such that at any given moment in time the wave-induced fluctuations of pore pressure are the same throughout the entire volume of rock under consideration. Under this condition, the local-flow (or squirt-flow) effect (e.g., Mavko and Jizba, 1991), as well as Biot's (1956) velocity-frequency dispersion are negligible.

If the rock is partially saturated with the liquid-phase saturation S, and saturation is homogeneous, the isostress Reuss (1929) average can be used for obtaining the effective bulk modulus of the pore fluid in eqns (2) and (3):

$$K_f^{-1} = SK_l^{-1} + (1-S)K_g^{-1}, \tag{4}$$

where K_l and K_g are the bulk moduli of the liquid and gas, respectively.

If saturation is patchy and the rock's dry frame is elastically homogeneous, the shear modulus is the same for dry and saturated patches because it is not affected by pore fluid. The volumetric fraction of the saturated patches is S and that of the dry patches is $1-S$. Then, following Packwood and Mavko (1995), we can use Hill's (1963) equation to find the effective bulk modulus K_{satP} of the volume, independent of the shape of the patches:

$$(K_{satP} + \tfrac{4}{3}G)^{-1} = S(K_0 + \tfrac{4}{3}G)^{-1} + (1-S)(K_l + \tfrac{4}{3}G)^{-1}, \tag{5}$$

where K_0 and K_l are the bulk moduli of the liquid- and gas-saturated rock, respectively:

$$K_0 = K_s \frac{\phi K_{dry} - (1+\phi)K_l K_{dry}/K_s + K_l}{(1-\phi)K_l + \phi K_s - K_l K_{dry}/K_s},$$

$$K_l = K_s \frac{\phi K_{dry} - (1+\phi)K_g K_{dry}/K_s + K_g}{(1-\phi)K_g + \phi K_s - K_g K_{dry}/K_s}. \tag{6}$$

If V_p and V_s are available at saturation S, K_{dry} can be found from eqns (5) and (6) as:

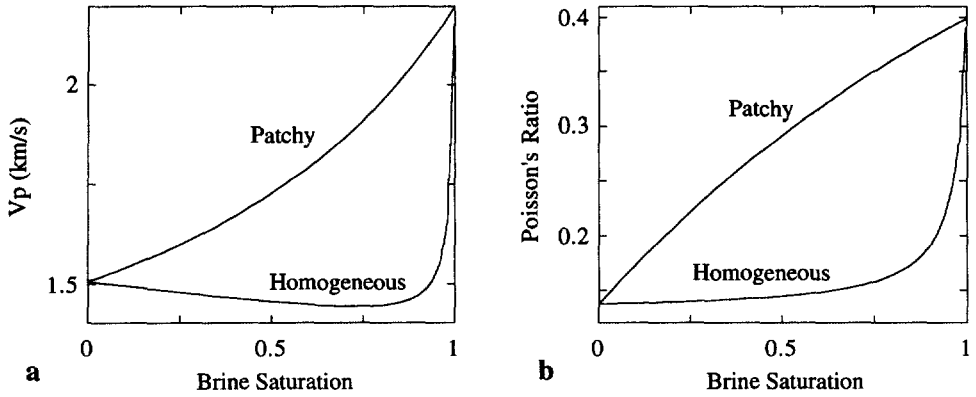

Fig. 3. Theoretical estimates of velocity (a) and Poisson's ratio (b) vs water saturation for homogeneous and patchy patterns in Ottawa sand. The properties of the dry frame are from Han (1986). The sample is saturated with brine and gas whose bulk moduli are 2.55 and 0.018 GPa, respectively. These numbers correspond to brine of salinity 30,000 ppm and methane at 10 MPa pore pressure and 50°C temperature (Batzle and Wang, 1992).

$$
\begin{aligned}
&K_{\text{dry}} = 0.5(-B+\sqrt{B^2-4AC})/A,\\
&A = cq+M(bq+cf), \quad B = pc+dq-M(aq-bp-df+ce), \quad C = dp-M(ap+de);\\
&a = S[(1-\phi)K_l+\phi K_s], \quad b = SK_l/K_s, \quad c = \phi K_s-(1+\phi)K_l-K_lG'/K_s,\\
&d = K_lK_s+(1-\phi)G'K_l+\phi G'K_s, \quad e = (1-S)[(1-\phi)K_g+\phi K_s], \quad f = (1-S)K_g/K_s,\\
&p = K_gK_s+(1-\phi)G'K_g+\phi G'K_s, \quad q = \phi K_s-(1+\phi)K_g-K_gG'/K_s;\\
&M = \rho V_p^2, \quad G' = 4G/3 = 4\rho V_s^2/3;
\end{aligned}
\tag{7}
$$

where G is the (independent of saturation) shear modulus of the rock, and M is the (compressional) M-modulus defined as the product of the bulk density and P-wave velocity squared.

In Fig. 3a we give an example of compressional-wave velocity changes in Ottawa sand with saturation, depending on the saturation pattern. If saturation is homogeneous, the compressibility of the water–air mixture is very close to that of air for almost all saturations. Only when water saturation approaches unity, does the compressibility of the mixture sharply decrease and approach that of water. In this case the bulk modulus of the rock is approximately constant for almost all saturations and sharply increases as the rock becomes fully saturated. At the same time, the density of the rock steadily increases with increasing saturation. This results in a slight V_p decrease with increasing saturation. Only at a very high saturation V_p approaches its value in the fully saturated rock. The situation is completely different if saturation is patchy. In this case V_p steadily increases with increasing saturation.

In Fig. 3b we plot the dynamic Poisson's ratio ν of Ottawa sand vs saturation. It is calculated from V_p and V_s as

$$
\nu = \frac{1}{2}\frac{V_p^2/V_s^2-2}{V_p^2/V_s^2-1} = \frac{1}{2}\frac{3K-2G}{3K+G}. \tag{8}
$$

It is clear that this elastic constant is even more sensitive to the saturation pattern than V_p. Therefore, Poisson's ratio may serve as an indicator of the saturation pattern.

3. IDENTIFYING SATURATION PATTERN

The dry-frame Poisson's ratio in relatively clay-free rocks rarely exceeds 0.2. Spencer *et al.* (1994) report that many unconsolidated sands from the Gulf of Mexico have dry-rock Poisson's ratios near 0.18, while other Gulf Coast reservoirs have these values as low

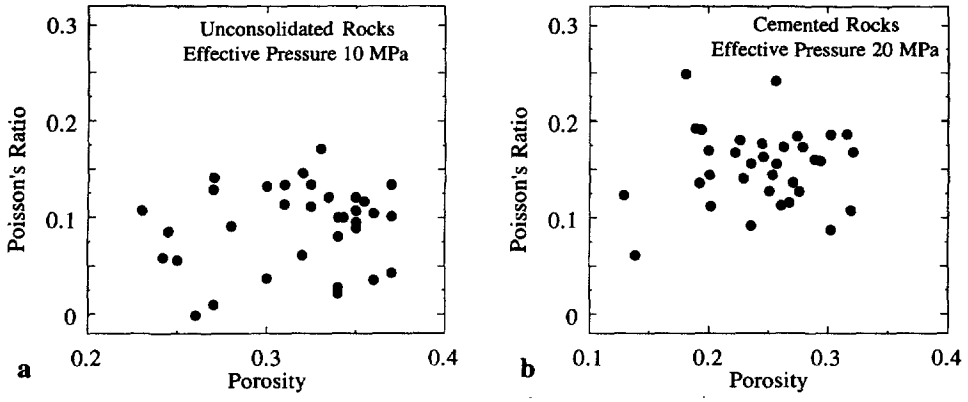

Fig. 4. Dry-frame Poisson's ratio vs porosity for (a) unconsolidated and (b) cemented high-porosity sandstones.

as 0.115. Only on several occasions (among a large number of rock samples) does the dry-rock Poisson's ratio exceed 0.2, with the maximum value 0.237. To illustrate this point, we plot dry-rock Poisson's ratios vs porosity (Fig. 4) for a suite of unconsolidated North Sea sands (Blangy, 1992) and for a suite of cemented high-porosity rocks (Strandenes, 1991). Based on these examples, we conclude that a reasonable range of the dry-frame Poisson's ratio variation is between zero and 0.2.

If velocity measurements on a saturated rock are available, we may use inversion eqns (2) and (7) to calculate the dry-frame elastic moduli assuming first that the saturation pattern is homogeneous and then that it is patchy. Next we can calculate the dry-frame Poisson's ratio for these two cases from eqn (8). Our working hypothesis is that if we use the wrong inversion technique (e.g., homogeneous inversion where saturation is patchy), the resulting dry-frame Poisson's ratio will fall outside the reasonable range thereby manifesting the saturation pattern.

To this end we propose the following saturation pattern identification scheme that can be applied, for example, to well log data.

- From the measured V_p and V_s and density find the bulk and shear moduli in the saturated rock using eqn (1).
- Using these moduli, known saturation value, and the properties of the gas and fluid phases, separately find the dry-frame moduli assuming first that saturation is homogeneous, eqn (2), and next that it is patchy, eqn (7).
- Find the dry-frame Poisson's ratio for these two cases using eqn (8).
- If the patchy inversion gives unreasonable values for the dry-frame Poisson's ratio, then the assumption that saturation is patchy is wrong, and, therefore, saturation is homogeneous. If the homogeneous inversion gives unreasonable values, then saturation is patchy.

Of course, in a realistic situation both homogeneous and patchy inversions may produce unreasonable Poisson's ratio values. In this case we recommend that the quality and interpretation of well log data be examined.

We test this method on a synthetic well log constructed from laboratory measurements of acoustic velocities and porosity in a suite of soft dry rocks from the Troll Field in the North Sea (Blangy, 1992). The effective pressure is 10 MPa. The liquid and gas bulk moduli are the same as in the example above (2.55 and 0.018 GPa, respectively). We assumed saturation values and saturation patterns vs depth (Fig. 5a) and calculated the "measured" velocities (Fig. 5b) accordingly, using eqns (3), (5), and (1).

We use these synthetic values to calculate the dry-frame Poisson's ratio first using the assumption that saturation is patchy in the whole depth interval and then that it is homogeneous (Fig. 6a). Obviously, the patchy-inversion Poisson's ratio may be quite unrealistic at some depth intervals. In order to identify saturation patterns, we clip the

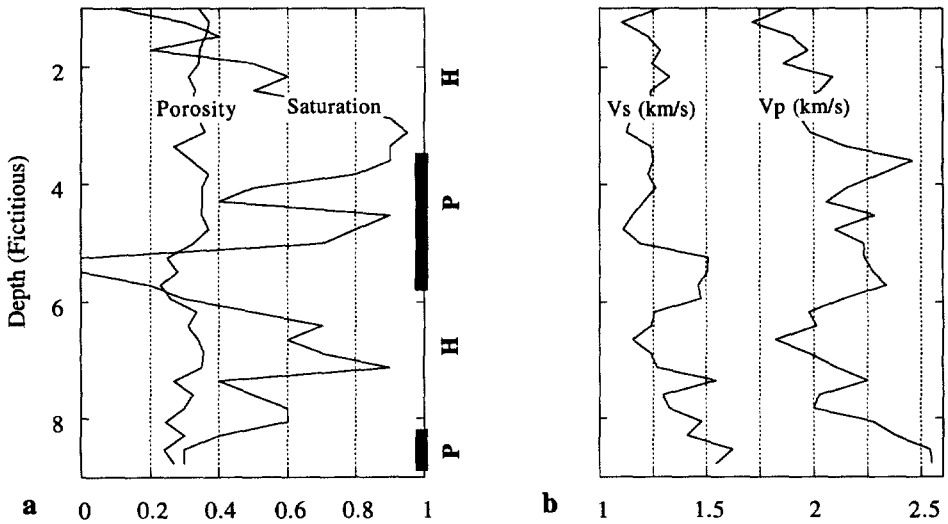

Fig. 5. Synthetic well log. a. Porosity and saturation vs depth. Bold vertical lines show depth intervals with patchy (**P**) saturation. The rest of the interval has homogeneous (**H**) saturation. b. Velocities calculated from dry-rock velocities and the assumed saturation values and patterns.

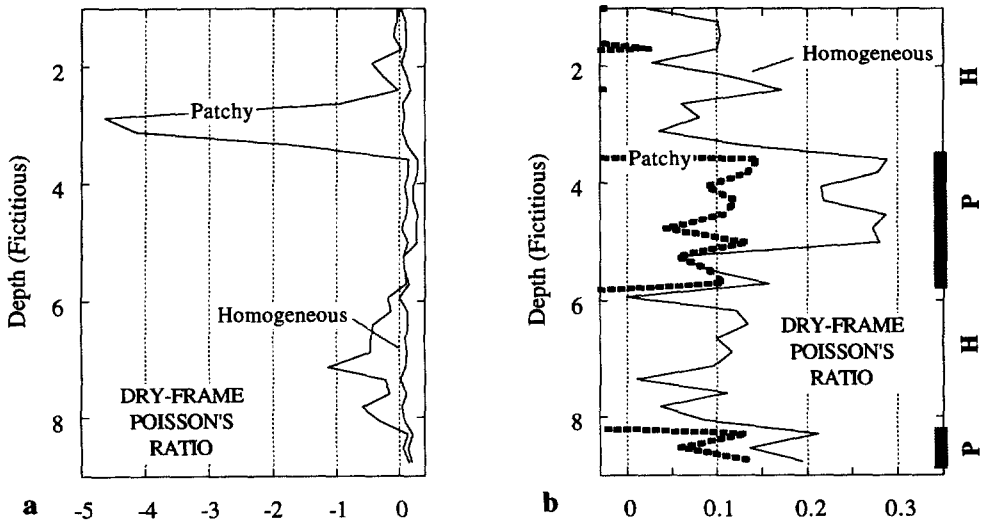

Fig. 6. Synthetic well log: inversion of the dry-frame Poisson's ratio. a. The whole range of the Poisson's ratio variation. b. Unreasonable Poisson's ratio values clipped. Bold vertical lines show depth intervals with patchy saturation.

calculated Poisson's ratio curve leaving out unreasonable negative values (Fig. 6b). What is left of the patchy-inversion curve most likely corresponds to the patchy saturation pattern. The rest of the interval corresponds to the homogeneous pattern. Notice that the homogeneous-inversion Poisson's ratio becomes unreasonably high in the patchy saturation domains. In the intervals where the correct inversion was applied, the produced dry-frame Poisson's ratios are exactly the input values (Fig. 7). The intervals of different saturation patterns thus identified exactly correspond to those in the original synthetic log.

If the saturation pattern is identified incorrectly, errors in calculating the dry-frame bulk modulus and *P*-wave velocity may be large (Fig. 8).

The proposed method can be successfully used only in soft rocks whose elastic moduli are very sensitive to the compressibility of the saturating fluid. The moduli of stiff rocks are not so sensitive to the pore fluid and neither are their Poisson's ratios. Consider, for example, two stiff sandstone samples, Fontainebleau and Beaver (Han, 1986). Indeed,

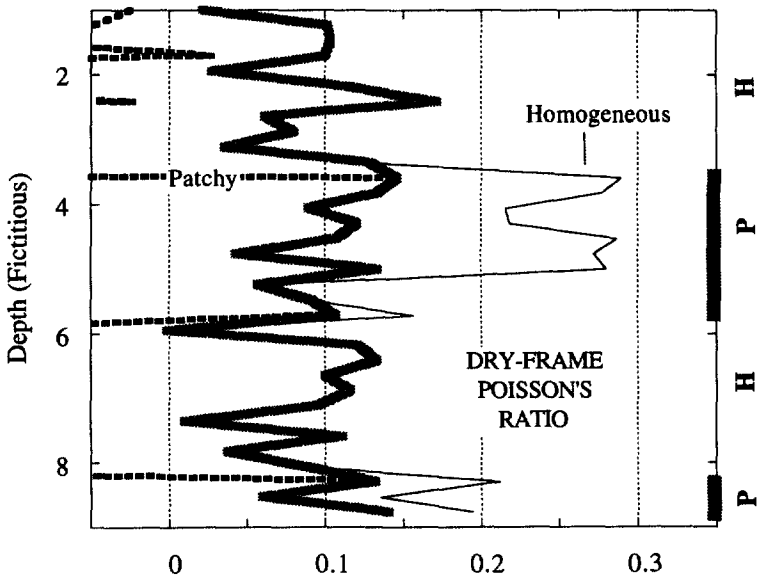

Fig. 7. Inversion of dry-frame Poisson's ratio vs depth. Bold gray line is for the true values.

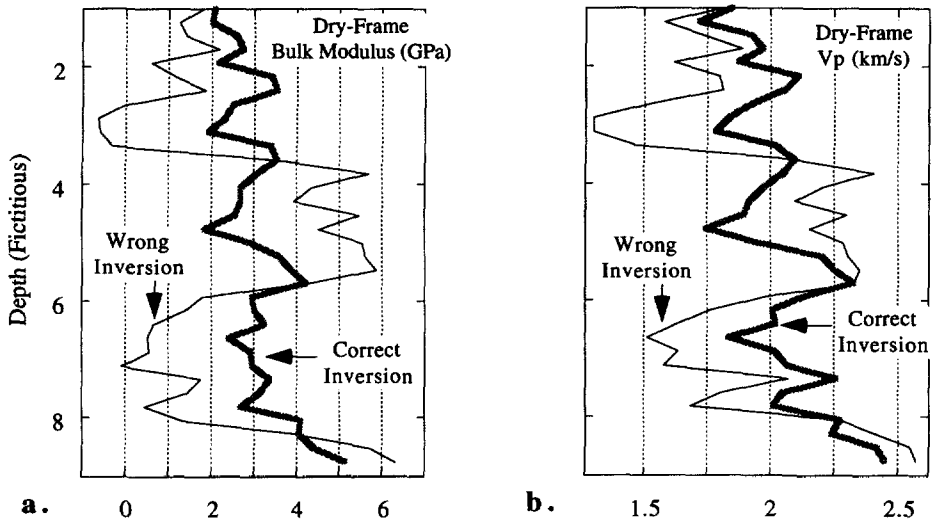

Fig. 8. Synthetic well log. a. Dry-frame bulk modulus. b. Dry-frame velocity.

their Poisson's ratios, independent of the pattern, stay within the reasonable range at all saturations (Fig. 9).

4. CONCLUSION

At a fixed partial saturation, two saturation patterns may exist in a rock volume: the homogeneous pattern where saturation is the same at any location in the volume, and the patchy pattern where a fully saturated patch may be surrounded by a dry region. It is important to identify the saturation pattern in order to correctly compute the dry-rock elastic moduli from *in situ* measurements. A synthetic examples show that the identification method where the dynamic dry-rock Poisson's ratio (from acoustic velocity measurements) is computed separately, based on the assumptions that the pattern is patchy, and that it is homogeneous, works in unconsolidated sands. This method is not likely to work in stiff rocks whose elastic moduli are not very sensitive to the pore fluid compressibility.

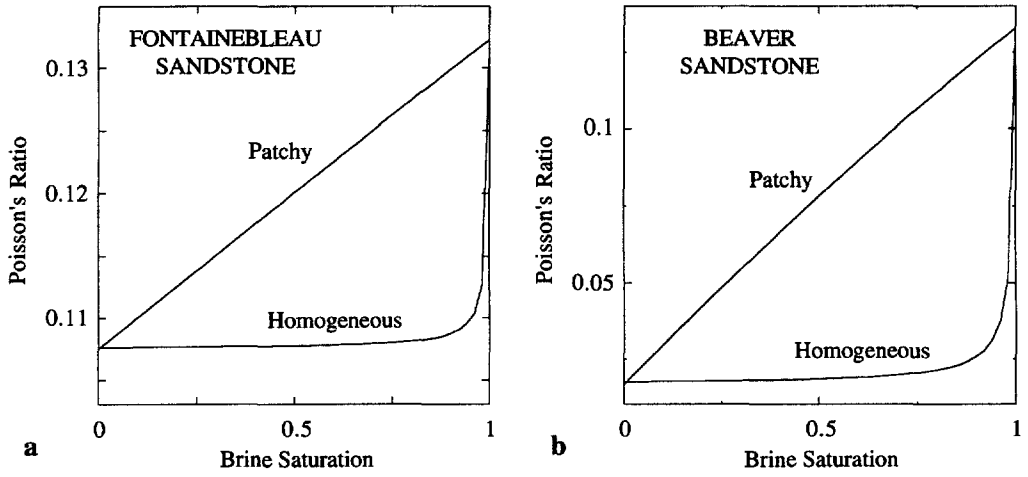

Fig. 9. Poisson's ratio vs water saturation for homogeneous and patchy patterns in (a) Fontainebleau and (b) Beaver sandstones. The properties of the dry frame are from Han (1986). The samples are saturated with brine and gas whose bulk moduli are 2.55 and 0.018 GPa, respectively.

Acknowledgement—This work was supported by DOE (Office at Basic Energy Sciences) and by the Stanford Rock Physics Laboratory.

REFERENCES

Batzle, M. and Wang, Z. (1992) Seismic properties of pore fluids. *Geophysics* **57,** 1396–1408.

Blangy, J. P. (1992) Integrated seismic lithologic interpretation: The petrophysical basis. Ph.D. thesis, Stanford University.

Biot, M. A. (1956) Theory of propagation of elastic waves in fluid saturated porous solid. I. Low frequency ranges. *J. Acoust. Soc. Am.* **28,** 168–191.

Cadoret, T. (1993) Effet de la saturation eau/gaz sur les propriétés acoustiques des roches. Ph.D. thesis, University of Paris.

Chatenever, A. and Calhoun, J. C. (1952) Visual examinations of fluid behavior in porous media—Part 1. *AIME Petroleum Transactions* **195,** 149–195.

Gassmann, F. (1951) Elasticity of porous media (Uber die elastizitat poroser medien), *Vierteljahrsschrift der Naturforschenden Gesellschaft, Zurich* **96,** 1–23.

Han, D.-H. (1986) Effects of porosity and clay content on acoustic properties of sandstones and unconsolidated sediments. Ph.D. thesis, Stanford University.

Hill, R. (1963) Elastic properties of reinforced solids: Some theoretical principles. *Journal of the Mechanics and Physics of Solids* **11,** 357–372.

Knight, R., Dvorkin, J. and Nur, A. (1998) Acoustic signatures of partial saturation. *Geophysics* **63,** 132–138.

Mavko, G. and Jizba, D. (1991) Estimating grain-scale fluid effects on velocity dispersion in rocks. *Geophysics* **56,** 1940–1949.

Packwood, J. and Mavko, G. (1995) Seismic signatures of multiphase reservoir fluid distributions: application to reservoir monitoring. Paper RP2.3, SEG 65th Annual Meeting, Expanded Abstracts, SEG, 910-913.

Reuss, A. (1929) Berechung der fliessgrense von mischkristallen auf grund der plastizitatbedingung fur einkristalle. *Zeitschrift fur Angewandte Mathematik und Mechanik* **9,** 49–58.

Spencer, J. W., Cates, M. E. and Thompson, D. D. (1994) Frame moduli of unconsolidated sands and sandstones. *Geophysics* **59,** 1352–1361.

Strandenes, S. (1991) Rock physics analysis of the Brent Group Reservoir in the Oseberg Field, Stanford Rock Physics and Borehole Geophysics Project, Stanford University.

Yin, H. (1993) Acoustic velocity and attenuation of rocks: Isotropy, intrinsic anisotropy, and stress-induced anisotropy. Ph.D. thesis, Stanford University.